


## OPTICAL ROUGHNESS CALCULATION FOR MATERIAL STRUCTURAL ANALYSIS OF ENERGY STRUCTURE APPLICATIONS UNDER DC PLASMA PROCESSES

**Alper Pahsa\***

Graduate School of Natural and Applied Sciences, Ankara Yıldırım Beyazıt University

Ankara, Türkiye, [apahsa@gmail.com](mailto:apahsa@gmail.com)

 <https://orcid.org/0000-0002-9576-5297>

*Article history: Received 8 August 2023, Received in revised form 22 August 2023, Accepted 19 September 2023, Available online 24 September 2023.*

### Highlight

Material structural reliability for low-dc plasma materials is determined by Weibull reliability predictions with surface roughness properties of materials in the determination of TOKAMAK fusion reactor structural design issues.

### Abstract

Surface qualities make aluminium a low-DC plasma interaction candidate. Aluminum for energy system structure building is studied experimentally, with observations obtained. Aluminum is cheap and frequently utilized in aerospace applications. The selection of materials for new applications of thermonuclear fusion energy, such as Tokamak reactor walls and fusion-based spaceship thrust structures, is important to decide in the design phase. In this study, an experimental setup application is created with low DC-type He plasma ions processed on aluminium pellet surfaces. The physical changes of the aluminium pellet material as an example of an energy structure surface are analysed under a scanned array microscope and 3D surface plots to detect optical roughness attributes.

### Keywords

Tokamak reactors; plasma material interaction; sputtering; 3DSurface Plot; optical roughness.

### Introduction

Aluminum (Al) material is found in increasing usage in automotive, aerospace, defence, and energy industrial applications. The main reason to thrust Al is its strength-to-weight ratio, together with its good casting ability and machinability. Aluminum is a lightweight material with a density of  $2.7 \text{ g/cm}^3$ . Pure aluminium and its alloys have a face-centred cubic (fcc) structure. It is stable at a melting point of  $657^\circ\text{C}$ . Because the fcc structure includes multiple slip planes, this crystalline structure affects the excellent formability of Al alloys.



Figure 1. Pure Aluminum Metal Ore. *Source: [1].*

Though aluminium is a thermodynamically reactive material, it has good corrosion resistance. Because of the formation of a compact and adherent oxide film on the surface, it is used in many applications in structures in building construction, power lines, transportation fields, food, and the chemical industry. However, in aggressive environments, such as high-temperature plasma, space environments, and/or petroleum environments, aluminium surfaces can be subjected to many surface changes due to wear and erosion. One of

the most important considerations to minimize the cost in industry is to make it possible to decrease equipment downtime [2]. Energy systems and space applications Fusion reactors are ideal for energy production. It is an ideal application without radioactivity, and it has an endless fuel source. In fusion energy reactors, nuclear fusion reactions in the core plasma generate energetic particle sets, including He and neutrons for H-based fuels [3]. If two nuclei combine to form a single, larger nucleus, a process called nuclear fusion occurs. That process is blocked by Coulomb repulsion, which acts to prevent the two positively charged particles from coming close enough to be within range of their attractive nuclear forces and "fusing". The range of the nuclear force is short, hardly beyond the nuclear "surface", but the range of the repulsive Coulomb force is long, and that force thus forms an energy barrier. The height of this Coulomb barrier is related to the charges and the radii of the two interacting nuclei. For two protons, the barrier is 400 keV. With respect to highly charged particles, it is certain that the barrier is correspondingly higher. This formation is generally seen in plasma environments. Plasma is an electrically conducting fluid that is electrically neutral from the outside, in which ions and electrons move independently of each other. In fusion reactors submerged in a magnetic field, ions and electrons move on a helical trajectory winding around field lines and will be forced to move along the field. This is the magnetic confinement principle on which TOKAMAK fusion reactors are based [4]. Nuclear fusion also offers many opportunities for space applications. The future of nuclear technology for space exploration promises even more remarkable journeys and amazing discoveries. Future space missions will need increased power for propulsion and surface power applications to support both robotic and human space exploration missions. However, in normal fusion reaction operations, magnetic confined reactor structures or nuclear electric propulsion system structures are exposed to neutronic, thermal, radiative, and thermomechanical stress loading. Moreover, the management of the interface between the plasma and the wall structures is critical [5]. Furthermore, the main results obtained concerning confinement, like H mode, were based on efficient management of this interface. Several types of phenomena may enter play at the wall, for instance, the absorption of large quantities of gas issued by the plasma, erosion due to the action of fast particles, and heating (the heat flux can reach several megawatts per square meter). This process causes plasma radiation to lose a significant quantity of temperature and the type of impurities that plasma contains. This process causes the plasma wall to deteriorate over time and to release neutrons into the environment [3,6–16]. The interaction of plasma with the reactor walls has been one of the critical issues in the development of fusion energy reactors because plasma-induced erosion can seriously limit the lifetime of the wall components [17–19]. Therefore, in space applications, plasma-facing structures must be designed to minimize this type of effect and to withstand particles and radiation from the plasma.

In the literature, there are many studies related to plasma-tokamak reactor structural material interactions. In divertor sections, rising He ash measurements in ITER or DEMO-type reactors are stated. Studies reflect the effects of alpha particle concentration on plasma processes, and the calculations are given as zero-dimensional power and particle balance equations. As a result of this, fusion reactions and optimum conditions are investigated. The studies also show that hydrogen ash because of the deuterium-tritium reaction cannot be avoided in fusion. In respect to ITER and DEMO class reactors, experimental work underlines the importance of low-activation materials such as steel, SiC ceramic composites, and vanadium alloys in the material selection of the reactors resistant to fusion sputtering. As new materials are found in these investigations, new types of diagnostic tools and measurement techniques are also included [4,20,21]. In this study, Al material is selected as a candidate material for energy system structures in reactor wall structures, either in reactors or in space applications. In the experiment setup, a plasma of He ions is generated at a high DC voltage and low temperature. The generated plasma is directed at an aluminium target, and the deformation of the target is analysed as a function of interaction time. Then the aluminium target pellets surface roughness is physically observed under a scanning electron microscope, the images are analysed to derive the optical roughness of the surface of the metal image, and their surface plot mesh graph is drawn. So that created optical roughness information can be used in calculating the structural reliability calculations in future studies. This study brought a new perspective to the derived fault data by using the optical roughness parameters in future structural reliability calculations. So that the structural reliability calculations of the Tokamak fusion reactor will be made in a cost-effective manner.

## Methods

In the experimental study, a setup was designed for the plasma-wall interaction. This setup helps to observe the plasma wall interaction and the plasma-surface interaction. Moreover, deformations on the surface are observed, and the material reliability of the target is calculated. The experimental setup schema considered in the work is shown in figure 2. In this setup, the air in the vacuum-able plasma boiler tube was initially evacuated

with the help of a vacuum pump. Then he flowed into the tube, and plasma was obtained by ionizing the gas inside with the high DC voltage applied between the cathode and the anode made up of Al. The effect of plasma and the surface of the Al anode and cathode plates are interacted. The physical effects of these plates were investigated. In the study, it was originally designed to make the plasma boiler tube from Al, but because of insulation problems and the possibility of arcing, the Al boiler was abandoned, and a quartz boiler (tube) was produced. Since the aim of the work is to concentrate on the physical surface effects on the Al anode and cathode surfaces, the Langmuir probe is not applied in the experiment. The same amount of vacuum and hydrogen gas is fed into the boiler as a control point in the experiment. So that the measurement of the plasma density in the tube was not observed.

The plasma beam is produced under high DC potential in the experimental setup given in figure 2. A 10 kV DC voltage source is applied between cathode and anode to ionize He in an evacuated glass hollow tube. The produced He ions and ejected electrons are then struck onto aluminium plates placed at the anode and cathode, respectively. The distance between the anode and cathode plates is placed at 5 cm to get plasma, as seen in figure 3. He plasma is generated by vacuuming the quartz tube many times until it reaches a 10 - 3 Torr vacuum and is filled fully with He gas. This process is repeated 5 - 6 times until the tube is free of air and the inside of the tube is filled with hydrogen gas from the input end. After the process to stabilize the hydrogen gas inside the quartz tube, a small pipe is connected to the exit end. This pipe of the quartz tube is put into the water-filled container. This is provided that stabilized He gas reside inside the quartz tube and that, at the same time, He gas flow is given at the input end of the quartz tube at 100 ml/min under atmospheric pressure. The used He gas was 99.9% pure, and the total gas flow rate was 100 ml/min.

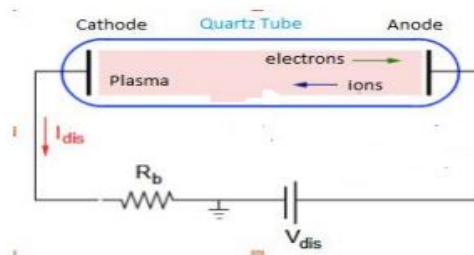


Figure 2. Experimental Setup Schema. Source: [16].



Figure 3. Generated He Plasma.

For the experiment, six aluminium pellet samples were made. Each time, two plates were placed at the cathode and anode, respectively, and subjected to the radiation for a time value of 60, 120, 180, 240, 300, and 360 minutes. The anode and cathode surfaces are affected by the He plasma. A Field Emission Scanned Electron Microscope (HITACHI SU5000 Scanned Field Emission Scanned Array Microscope) is used to display the detailed surfaces of the Al pellet surfaces at the final stage. SEM measurements are performed at room temperature (25°C). For anode and cathode, grey-scale value images are produced for different magnification scales under SEM. These images are used to calculate the following optical roughness parameters, respectively:

- Ra: Arithmetical mean deviation.
- Rq: Root means square deviation.

- Rku: Kurtosis of the assessed profile.
- Rsk: Skewness of the assessed profile.
- Rv: Lowest valley (given by the min measurements).
- Rp: Highest peak (given by the max measurements).
- Rt: The total height of the profile.

The above parameters are calculated for each SEM image for the anode and cathode of the pellet for different He plasma process times. The above optical roughness parameters were calculated using the open-source application Image [22]. It is a widely used research application in scientific image processing studies. Also, a surface mesh plot is performed for the surface images under SEM to see the peaks and valleys of the image. Table 1 shows the Al anode and cathode samples that are irradiated with He plasma with different time processes and SEM image optical roughness parameters. In Table 1, optical roughness parameter values are going to be used in the three-parameter Weibull formula in the future for calculating the reliability of the Al under He plasma.

Table 1. He Plasma Al plate SEM Image Optical Roughness Failure Data Set.

Sample Image Label	Ra	Rq	Rku	Rsk	Rv	Rp	Rt
60 min,2mm, Cathode	146.699	144.636	1.047	1.139	255	65	320
60 min, 500nm, Cathode	94.475	87.323	1.221	1.675	255	15	270
60 min,1µm, Cathode	91.764	84.420	1.313	2.114	255	3	258
60 min,3µm, Cathode	96.324	89.212	1.270	1.905	255	0	255
60 min,10µm, Cathode	95.300	88.055	1.298	2.035	255	0	255
60 min,50µm, Cathode	90.370	80.283	1.433	2.533	255	0	255
240 min,2mm, Cathode	126.826	125.879	1.025	1.080	255	74	329
240 min,50µm, Cathode	119.681	110.727	1.237	1.731	255	0	255
240 min,10µm, Cathode	104.405	96.393	1.266	1.866	255	0	255
240 min,3µm, Cathode	103.252	94.389	1.302	2.003	255	0	255
240min,500mm, Cathode	78.738	71.791	1.296	2.060	255	0	255
360 min,2mm, Cathode	128.992	127.426	1.039	1.119	255	76	331
360 min,50µm, Cathode	76.864	69.235	1.470	2.908	255	0	255
360 min,10µm, Cathode	97.095	89.890	1.307	2.094	255	0	255
360 min,3µm, Cathode	94.678	87.759	1.278	1.969	255	0	255
360 min,1µm, Cathode	93.285	86.242	1.284	1.977	255	0	255
360 min,500nm, Cathode	79.299	71.734	1.342	2.218	255	0	255
120 min,2mm,Anode	151.888	149.898	1.041	1.117	255	61	316
120 min,500mm,Anode	88.241	81.285	1.263	1.877	255	0	255
120 min,1µm,Anode	85.792	79.167	1.254	1.868	255	0	255
120 min,5µm,Anode	96.291	89.742	1.308	2.148	255	0	255
120 min,10µm,Anode	95.707	88.797	1.314	2.146	255	0	255
120 min,50µm,Anode	93.920	84.694	1.432	2.613	255	0	255
180 min,2mm,Anode	155.080	152.316	1.054	1.152	255	75	330
180 min,50µm,Anode	89.547	79.882	1.361	2.170	255	0	255
180 min,10µm,Anode	92.543	85.033	1.279	1.908	255	12	267
180 min,3µm,Anode	96.664	90.163	1.222	1.700	255	23	278
180 min,1µm,Anode	96.032	89.726	1.211	1.662	255	16	271
180 min,500nm,Anode	94.741	88.636	1.218	1.702	255	33	288
300 min,50µm,Anode	95.030	83.355	1.422	2.423	255	0	255
300 min,10µm,Anode	95.236	88.178	1.259	1.849	255	0	255
300 min,5µm,Anode	96.201	89.345	1.237	1.761	255	0	255
300 min,3µm,Anode	96.074	89.421	1.227	1.720	255	0	255
300 min,500nm,Anode	95.245	88.992	1.212	1.670	255	5	260
300 min,1µm,Anode	98.728	92.601	1.207	1.655	255	14	269
300 min,10µm,Anode	95.276	88.177	1.275	1.937	255	0	255

## Results and discussion

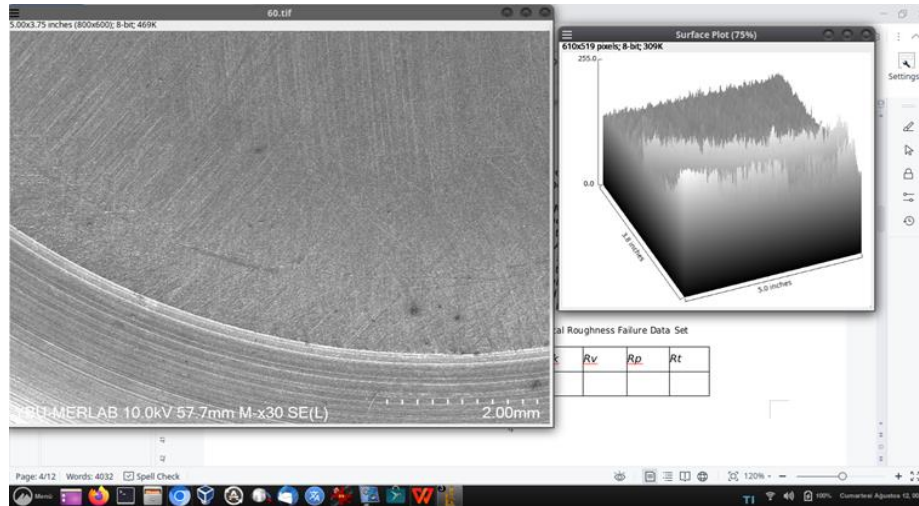
Figure 4 displays physical surface plots and grey scale views of SEM on the surface of Al samples at the anode and cathode at 60, 180, 200, 240, 300, and 360 minutes under He plasma interaction. In these sample fields

of grains, black points and semi-grey spots are seen. SEM surface plots showed hills (high areas) and holes (low areas) on the Al pellet surfaces. The material reliability will be calculated with optical roughness parameters at Al anode pellets and cathode pellets to make comparisons as in reliability graphs. These results will show the status of the surface attributes of the optical roughness measures. So that material selection criteria will be determined for plasma-based energy structures such as fusion Tokamak reactors or space thrust systems based on fusion architecture.

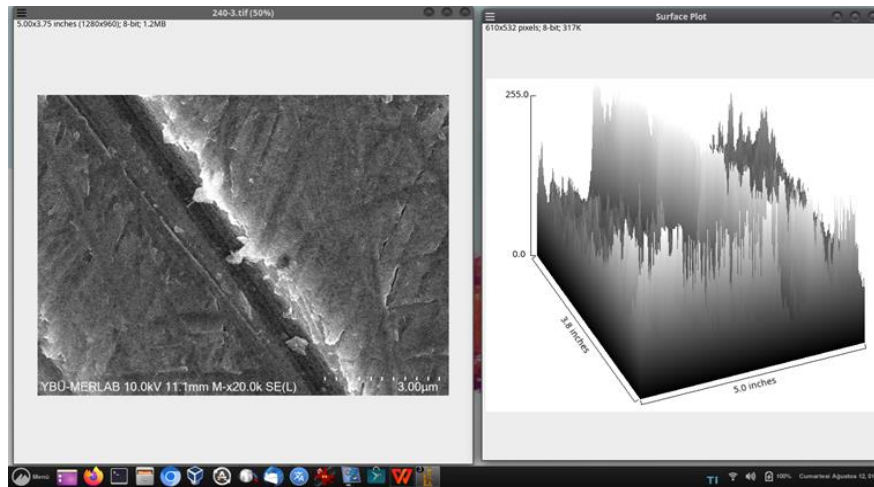
**Sample Image Label**

**SEM Image Views and Surface Plots of the SEM Images**

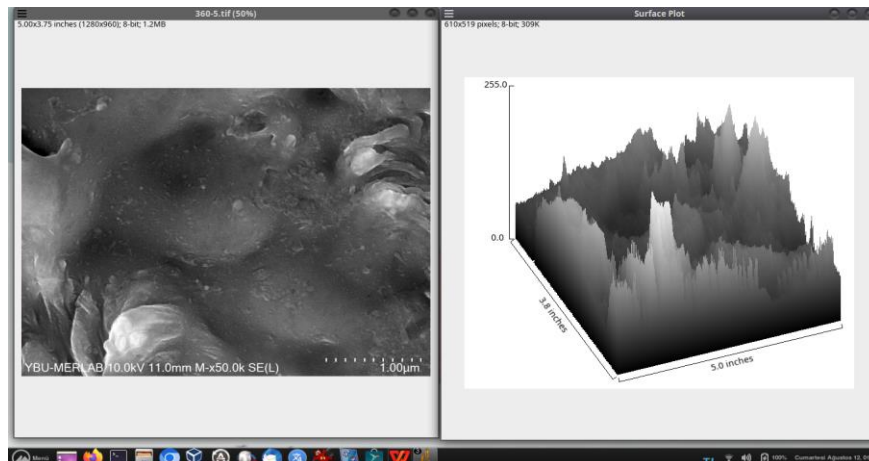
60 min, 2mm, Cathode



240 min, 3µm, Cathode

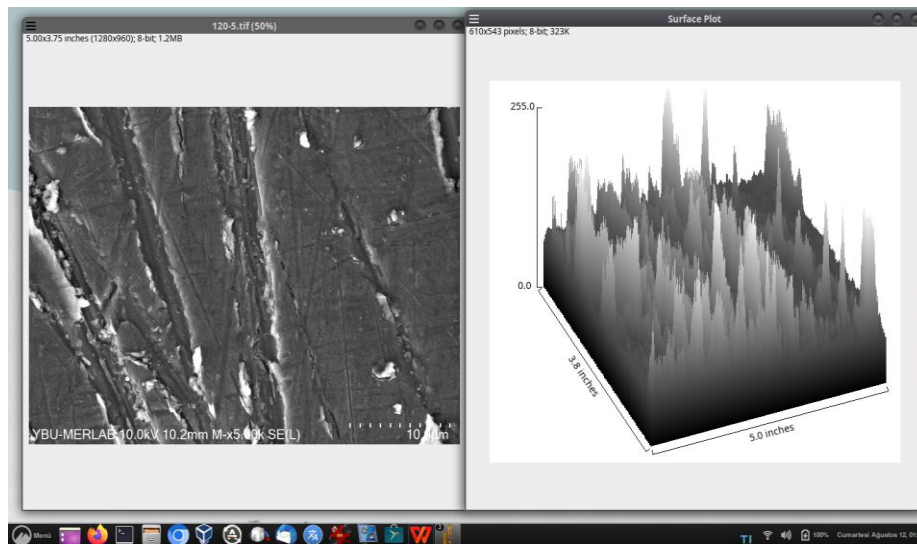


360 min, 1µm, Cathode





120 min, 10 $\mu$ m,  
Anode



300 min, 50 $\mu$ m,  
Anode

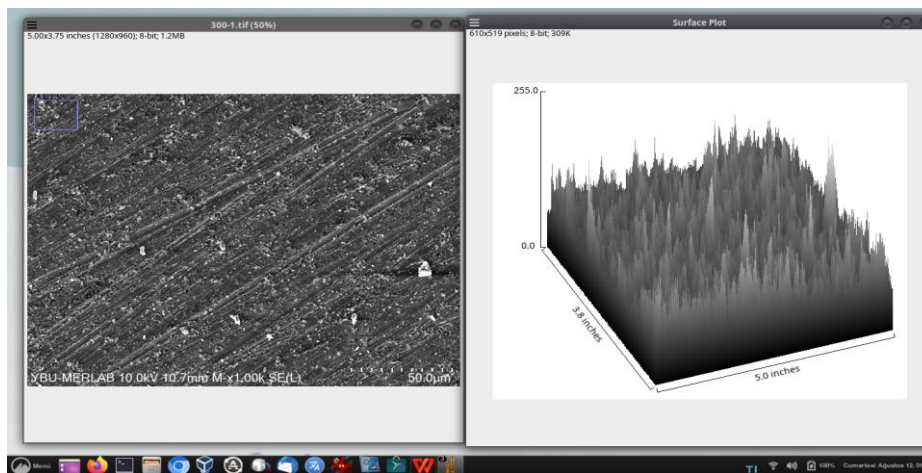


Figure 4. SEM AI surface observation images and their 3D surface of anode and cathode pellets with different process time under He plasma.

Based on the above findings, the observations given in Table 1 are compared with the findings given in [23]. According to [23], the study is performed under an atomic force microscope (AFM) and precisely measured, and the process is based on ASME B46.1 standard-defined terms Sa and RMS values. According to the ASME B46.1 standard, Sa (surface roughness) and RMS (root mean square) both represent surface roughness, but each is calculated differently. Sa is calculated as the roughness average of a surface's measured microscopic peaks and valleys. RMS is calculated as the root mean square of a surface measured by microscopic peaks and valleys. In the study above, ImageJ software is used on the SEM images for different plasma processing times to determine the optical roughness characteristics.

Using Table 1 and the study [23], the following graphs are generated for the common process times given in both methods:

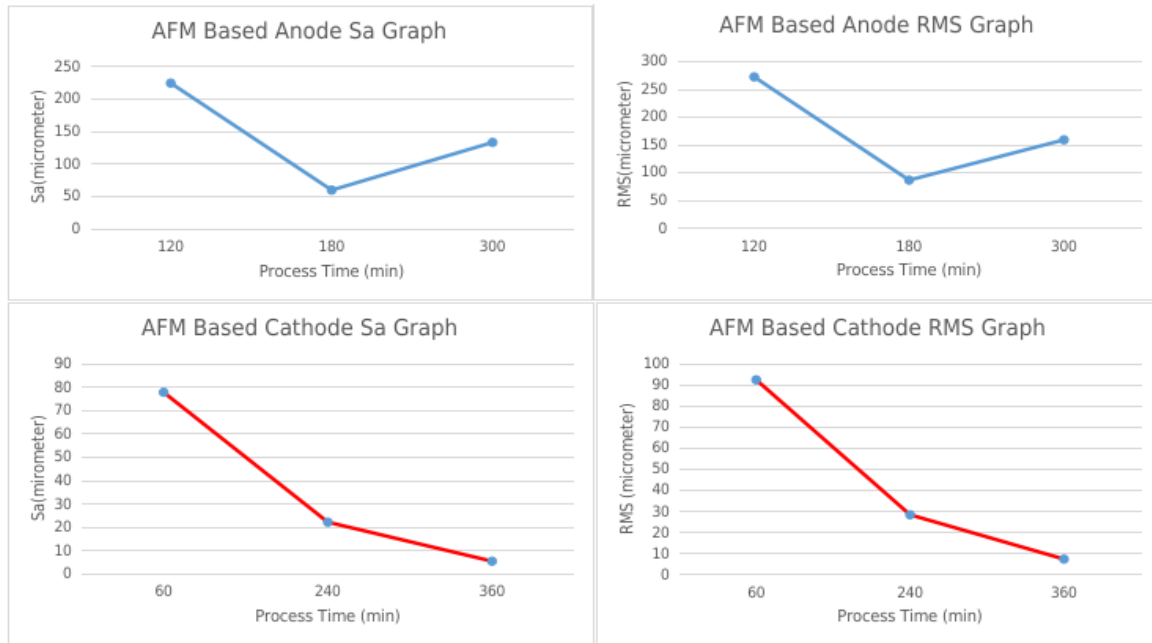


Figure 5. AFM Measured RMS and Sa Graphs of Anode and Cathode Surface Pellets Based on Different Process Times (min).

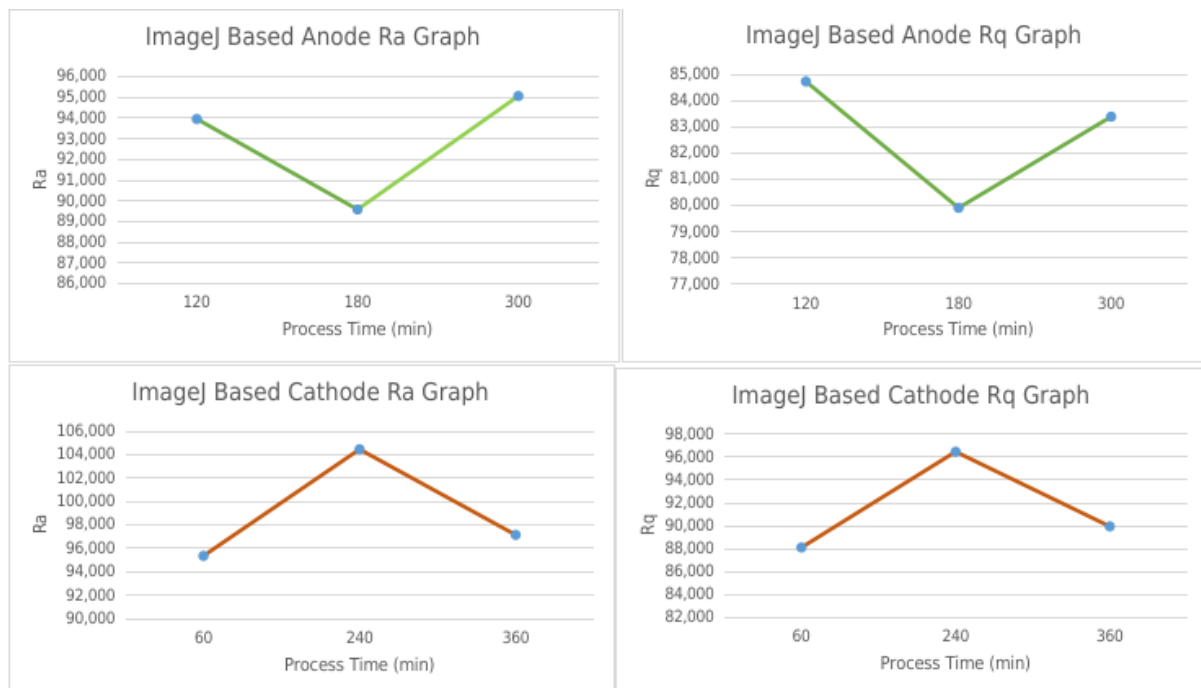


Figure 6. ImageJ Software Measured Rq and Rq Graphs of Anode and Cathode Surface Pellets Based on Different Process Times (min).

The same graphs are produced based on the Table-1 values for specified process times of the AFM measurements of anode and cathode pellets. In this case, the measured optical roughness values are Ra and Rq values measured under ImageJ software SEM images. The given figure 6 shows the anode and cathode surfaces of Ra and Rq at the specified process times as given in figure 5. The two measurements are compared by using the correlation function to determine if Ra values can be used for Sa and Rq values can be used for RMS. The correlation function is a statistical measure of strength used to determine the linear relationship between two variables. When the correlation of the two series is input, the correlation function then maps the output range between  $-1$  and  $1$ . A correlation coefficient of  $-1$  determines a perfect negative or inverse correlation, and a correlation coefficient

of 1 shows a perfect positive correlation. If the correlation coefficient shows 0, then there is no linear relationship between the values. To calculate the correlation, each series is determined by calculating the standard deviation and the covariance between them. The correlation coefficient is covariance divided by the product of the two variables' standard deviations [24].

Table 2. He Plasma Al Anode and Cathode Plates AFM Measurements (Sa and RMS) and ImageJ Calculations (Ra and Rq) Correlation Results.

Correlation Table	AFM Measurement of Anode for Sa	AFM Measurement of Anode RMS	AFM Measurement of Cathode for Sa	AFM Measurement of Cathode RMS
ImageJ Measurement of Anode Ra	0.711678358			
ImageJ Measurement of Anode Rq		0.92994807		
ImageJ Measurement of Cathode Ra			-0.468889172	
ImageJ Measurement of Cathode Rq				-0.474880479

According to Table 2, AFM measured anode Sa and RMS values, and ImageJ calculated Ra and Rq values for the same processing times, showing a positive correlation above 0. AFM measured cathode Sa and RMS ImageJ calculated Ea and Rq values are negatively correlated.

### Impact

This study provides a cost-efficient methodology for comparison method criteria to determine the material selection in designing Tokamak fusion reactors for future reactor wall structures. This method can be used to directly calculate different material optical characteristics for library generation so that the designers of future fusion reactors can use this bias to create the best match for their blueprints. This phenomenon will be used in designing economic budgets for the Tokamak fusion reactor's construction to underline productivity, efficiency, durability, and sustainability cost factors of the reactor's structural and operational lifetime.

### Conclusions

From the results given above, optical roughness parameters are analysed by using image processing techniques on the surface structures of materials. According to the observations given in the results section, it is clearly determined that the ImageJ calculated optical roughness parameters can be used for anode pellets; however, in the cathode section, it is observed that there is a negative correlation that the calculated optical roughness parameters show unsatisfactory results. The reason for the negative correlation given in cathode pellet calculations for optical roughness parameters is that the original SEM images of the cathode pellets sampling size should be increased, and more images must be taken with the SEM. Another solution to increase the positive correlations between AFM measurements is to use metal microscope taken images to take more sample images from cathode pellets to increase the measurement samples and determine a satisfactory relationship for future uses. It is also expected to be a difference between the anode and cathode surfaces under the plasma process. This can be observed from the optical roughness parameters when compared with the AFM measurements for anode and cathode surfaces. Optical roughness measurement shows a promising method for future usage in material reliability calculations when precise sampling and calculations are performed during the experiments for future studies. This method is already used in different sectors of the manufacturing industry for quality control purposes. By spreading this technique to be used in the energy industry for material selection, it will achieve a cheap solution and cost-efficient method for the aviation and defence industries for calculating structural reliability predictions. In reliability literature, it is widely known that material structural reliability is investigated using five methods. These are material selection, reliability analysis, maintenance and inspection, heat and stress, and erosion and damage. In the literature, the structural reliability of Tokamak fusion reactors is not studied based on the values of the huge fusion reactor experiments. Construction and design of the Tokamak fusion reactors are focused on building costs. However, maintenance and material resilience are other questions that need to be asked during the operation. To calculate operational costs, an expert should consider material life cycle costs and maintenance costs for a fusion reactor's resilience. Material life cycle costs are directly tied to the material reliability data that must be known during construction and operation. In this respect, no special study is found in the literature with



respect to fusion reactors. Only commercial plasma reliability studies that are found in the literature are based on surface coating. This is not satisfactory in the determination of the structural reliability data for fusion reactors. In reliability data, faults need to be known as properties of the investigated subject. In this respect, fatigue, crack, and deformation information can be used to show the reliability of structural material studies of fusion reactors. This work's results will be used in calculating the optical roughness information for material directly from the fault data under a plasma processing activity, and this direct information can be used in predicting the characteristic curve of the material structure based on the Weibull Prediction method. As this statistical information is found, for candidate structural materials that are selected for fusion reactor construction, the life cycle time of the designed material will be known by using its measured surface roughness data over time specific to the selected material. Knowing the life cycle time of the material, the operational costs of the selected material will be determined. As a result, fusion reactor construction costs will be calculated directly during the planning phase of the construction work.

### Conflict of interest

During the study of the work, no potential financial or non-financial conflict of interest existed. Also, with the study, no informed consent of human participants and/or animals was used, and the study complied with the widely accepted ethical codes of world-accepted research rules, guidelines, and literature standards.

### Acknowledgments

Author would like to thank to The Scientific and Technological Research Council of Turkey (TUBITAK) in supporting of this study.

### References

- [1] Xometr Inc., Aluminum: History, characteristics, types, properties and applications, (2023). <https://doi.org/https://www.xometry.com/resources/materials/what-is-aluminum/>.
- [2] S. Pirizadhejrandoost, M. Bakhshzad Mahmoudi, E. Ahmadi, M. Moradshahi, The corrosion behavior of carburized aluminum using DC plasma, *J. Metall.* 2012 (2012) 1–4. <https://doi.org/10.1155/2012/258021>.
- [3] IAEA, Atomic and Plasma Material Interaction Data for Fusion, 13 (2007).
- [4] R. Alba, R. Iglesias, M.Á. Cerdeira, Materials to be used in future magnetic confinement fusion reactors: A review, *Materials (Basel)*. 15 (2022) 6591. <https://doi.org/10.3390/ma15196591>.
- [5] A. Pahsa, Modelling plasma material interactions in spacecraft magnetic fusion devices, in: 2019 9th Int. Conf. Recent Adv. Sp. Technol., IEEE, 2019: pp. 655–662. <https://doi.org/10.1109/RAST.2019.8767780>.
- [6] IAEA, Lifetime predictions for the first wall and blanket structure of fusion reactors, (1985).
- [7] J. Rafelski, S.E. Jones, Cold nuclear fusion, *Sci. Am.* 257 (1987) 84–89. <https://doi.org/10.1038/scientificamerican0787-84>.
- [8] L. Rajablou, S.M. Motevalli, F. Fadaei, Study of alpha particle concentration effects as the ash of deuterium-tritium fusion reaction on ignition criteria, *Phys. Scr.* 97 (2022) 095601. <https://doi.org/10.1088/1402-4896/ac831a>.
- [9] L. Conde, An introduction to langmuir probe diagnostics of plasmas, (2011) Figure-2, p.3. <http://plasmalab.aero.upm.es/~lcl/PlasmaProbes/Probes-2010-2.pdf>.
- [10] ASME B46.1:2019, Surface Texture (Surface Roughness, Waviness, and Lay)", NS-996086, Technical Standards ASME, (2020).
- [11] K. WojcZYkowski, New development in corrosion testing: Theory, methods and standards, AESF Found. *Plat. Surf. Finish.* (2011) 98.
- [12] IAEA, M. Kikuchi, K. Lackner, M.Q. Tran, Fusion physics, (2012) 20–21.
- [13] J.P. Freidberg, F.J. Mangiarotti, J. Minervini, Designing a tokamak fusion reactor—How does plasma physics fit in?, *Phys. Plasmas*. 22 (2015). <https://doi.org/10.1063/1.4923266>.
- [14] K. Miyamoto, Fundamentals of plasma physics and controlled fusion, (2011) 1–21. <https://doi.org/10.1088/0029-5515/38/4/701>.
- [15] C.M. Braams, P.E. Stott, Nuclear fusion: half a century of magnetic confinement research, *Plasma Phys. Control. Fusion*. 44 (2002) 1767–1767. <https://doi.org/10.1088/0741-3335/44/8/701>.
- [16] Y.A. Chang, G. Herdrich, C. Syring, Development of inertial electrostatic confinement in IRS, in: *Sp. Propuls. Conf.*, Rome, Italy, 2016.
- [17] V. Kotov, Particle conservation in numerical models of the tokamak plasma edge, *Phys. Plasmas*. 24 (2017). <https://doi.org/10.1063/1.4980858>.

- [18] J. Rapp, G. De Temmerman, G.J. Van Rooij, P.A. Zeijlmans Van Emmichoven, A.W. Kleyn, Plasma-facing materials research for fusion reactors at Fom Rijnhuizen, in: 15th Int. Conf. Plasma Phys. Appl. Rom. J. Phys., 2011: pp. 30–35.
- [19] M. Malo, A. Moroño, E.R. Hodgson, Plasma etching to enhance the surface insulating stability of alumina for fusion applications, *Nucl. Mater. Energy.* 9 (2016) 247–250. <https://doi.org/10.1016/j.nme.2016.05.008>.
- [20] S.M. Motevalli, N. Dashtban, M. Maleki, Determination of optimum conditions in ITER tokamak by using zero-dimensional model, *Indian J. Phys.* 95 (2021) 2211–2215. <https://doi.org/10.1007/s12648-020-01857-6>.
- [21] M. Reinhart, S. Brezinsek, A. Kirschner, J.W. Coenen, T. Schwarz-Selinger, K. Schmid, A. Hakola, H. van der Meiden, R. Dejarnac, E. Tsitrone, R. Doerner, M. Baldwin, D. Nishijima, W.P. Team, Latest results of eurofusion plasma-facing components research in the areas of power loading, material erosion and fuel retention, *Nucl. Fusion.* 62 (2022) 042013. <https://doi.org/10.1088/1741-4326/ac2a6a>.
- [22] C.A. Schneider, W. Rasband, K.W. Eliceiri, *Image processing and analysis in Java*, (2012).
- [23] A. Pahsa, Y. Aydoğdu, F. Gökteş, Mathematical calculation of material reliability using surface roughness feature based on plasma material interaction experiment results, *Ekspluat. i Niezawodn. – Maint. Reliab.* 25 (2023). <https://doi.org/10.17531/ein/169815>.
- [24] Centre for Innovation in Mathematics Teaching, 12 correlation and regression, 215–242. [https://www.cimt.org.uk/projects/mepres/alevel/stats\\_ch12.pdf](https://www.cimt.org.uk/projects/mepres/alevel/stats_ch12.pdf).